

EVOLUTION OF THE MAGNETIC FIELD IN AR 5747 AND ITS APPROXIMATION AS A LINEAR FORCE-FREE FIELD

Y.-J. MOON*

Korea Astronomy Observatory, Whaamdong, Yooseong-ku, Taejon, 305-348, Korea

H. S. YUN

Department of Astronomy, Seoul National University, Seoul 151-742, Korea

G. S. CHOE

Princeton Plasma Physics Laboratory, Princeton, NJ 08543-0451, USA

Y. D. PARK

Korea Astronomy Observatory, Whaamdong, Yooseong-ku, Taejon, 305-348, Korea

D. L. MICKEY

Institute for Astronomy, University of Hawaii, 2680 Woodlawn Drive, Honolulu, HI 96822-1839, USA

1. Introduction

It is generally believed that magnetic fields play a central role in solar eruptive phenomena such as flares and coronal mass ejections. The energy released through solar eruptive processes is considered to be stored in nonpotential magnetic fields. The magnetic energy is supplied to the corona either by plasma flows moving around magnetic fields in the inertia-dominant photosphere or by magnetic flux emerging from below the photosphere. Since measurements of magnetic fields at the coronal altitude are not available, magnetograms taken at the photospheric level have been widely used for studies of magnetic nonpotentiality in flare-producing active regions and are also used through extrapolation to compute coronal magnetic fields.

Several attempts have been made to identify the relationships between time variation of nonpotentiality parameters and development of solar flares (Hagyard *et al.*, 1984; Hagyard *et al.*, 1990; Wang *et al.*, 1996; Wang 1997). Moon *et al.* (1999c, Paper I) reviewed previous studies on magnetic nonpotentiality indicators and discussed the problems involved in them. Specifically, they studied the evolution of nonpotentiality parameters in the course of an X-class flare of AR 6919

* e-mail:yjmoon@boao.re.kr



using MSO (Meer Solar Observatory) magnetograms. They showed that the magnetic shear obtained from the vector magnetograms increased just before the flare and then decreased after it, at least near the δ spot region. Moon *et al.* (1999a) proposed a measure of magnetic field discontinuity, MAD, defined as Maximum Angular Difference between two adjacent field vectors, as a flare activity indicator. They applied this concept to three magnetograms of AR 6919 and found that the high MAD regions well match the soft X-ray bright points observed by Yokoh. It was also found that the MAD values increased just before an X-class flare and then decreased after it. This paper constitutes one of the series of studies on evolution of magnetic nonpotentiality associated with major X-ray flares, which are performed using MSO vector magnetograms.

Metcalf *et al.* (1995) studied MSO magnetograms of AR 7216, which are obtained from the observation of Na I 5896 spectral line, employing a weak field derivative method (Jefferies and Mickey, 1991) and concluded that the magnetic field of AR 7216 is far from force-free at the photospheric level. This method could underestimate transverse field strengths for strong field regions due to the saturation effect and calibration problems (Hagyard and Kineke, 1995; Moon, Park, and Yun, 1999b). Metcalf *et al.* (1991) used polarization data of Fe I 6302 line to compare two calibration methods: the weak field derivative method (Jefferies and Mickey, 1991) and the nonlinear least square method (Skumanich and Lites, 1987). They found that there are noticeable differences in magnetic field strength larger than $B \geq 1200$ G between the two methods.

On the other hand, Pevtsov *et al.* (1997) analyzed 655 photospheric magnetograms of 140 active regions to examine the spatial variation of force-free coefficients. In their results, some of the active regions show a good correlation between B_z and J_z , but others do not. It is very natural that the force-free coefficient varies depending on the active region in question even when the coefficient is more or less constant over the active region. Now we raise the question of whether a certain relation can be drawn between the force-free coefficient and the evolutionary stage of an active region. Among the selections by Pevtsov *et al.* (1997), AR 5747 is exemplary of showing a good correlation between B_z and J_z . Thus, we have taken AR 5747 as the object of our study.

The purpose of this paper is to examine the magnetic nonpotentiality of AR 5747 associated with solar flares and investigate the evolution of the linear force-free coefficient. For this study, we have used the magnetograms spanning three days obtained from full Stokes polarization profiles of MSO. In Section 2, a description is given of the observation and analysis of the vector magnetograms. Computation of

Table I. Basic observational parameters of AR 5747.

Data	Date	Time	Scan	Data Points	Coord.
AR5747 a)	20 Oct., 1989	17:41-18:50	5.656''	30×30	S26W07
AR5747 b)	21 Oct., 1989	19:20-20:16	5.656''	30×30	S26W22
AR5747 c)	22 Oct., 1989	18:27-19:41	5.656''	30×40	S26W33

nonpotentiality parameters and their evolutions in relation to flaring activities is presented in Section 3. In Section 4, we discuss the evolution of the active region field as a linear force-free field. Finally, a summary and conclusion are given in Section 5.

2. Observation and Analysis

For the present work, we have selected a set of MSO magnetograms of AR 5747 taken on Oct. 20–22, 1989. The magnetogram data were obtained by the Haleakala Stokes polarimeter (Mickey, 1985) which provides simultaneous Stokes I,Q,U,V profiles of the Fe I 6301.5, 6302.5 Å doublet. The observations were made by a rectangular raster scan with a pixel spacing of 5.6'' (low resolution scan) and a dispersion of 25 mÅ/pixel. Most of the analyzing procedure is well described in Canfield *et al.* (1993). To derive the magnetic field vectors from Stokes profiles, we have used a nonlinear least square fitting method (Skumanich and Lites, 1987) for fields stronger than 100 G and an integral method (Ronan, Mickey and Orral, 1987) for weaker fields. In that fitting, the Faraday rotation effect, which is one of the error sources for strong fields, is properly taken into account. The noise level in the original magnetogram is about 70 G for transverse fields and 10 G for longitudinal fields. The basic observational parameters of the magnetograms used in this study are presented in Table I.

To resolve the 180° ambiguity, we have adopted a multi-step ambiguity solution method by Canfield *et al.* (1993) (for details, see the Appendix of their paper). In the 3rd and 4th steps of their method, they have chosen the orientation of the transverse field that minimizes the angle between neighboring field vectors and the field divergence $|\nabla \cdot \mathbf{B}|$.

Table II. Basic information of the major X-ray flares observed in AR 5747 (Solar Geophysical Data).

ID	Date	Start(UT)	End	Max.	Coord.	Optical Class	X-ray Class
F1	20/10/89	21:30	22:03	21:34	S26W11	1N	M1.4
F2	21/10/89	01:53	02:06	01:55	S28W09	1N	M2.4
F3	21/10/89	06:40	06:49	06:43	S27W16	1N	M1.9
F4	21/10/89	23:54	24:00	23:56	S28W22		M3.1
F5	22/10/89	11:15	12:30	11:21	S27W26	SN	M1.5
F6	22/10/89	15:54	16:47	15:58	S28W28	SN	M1.3
F7	22/10/89	17:08	21:08	17:57	S27W31	2B	X2.9

3. Evolution of Magnetic Nonpotentiality

In the active region AR 5747, a number of flares took place including a 2B/X3 flare. In Table II, we summarize some basic features of major X-ray flares during the observing period.

Figure 1 shows the ambiguity resolved vector magnetograms obtained on Oct. 20 to Oct. 22, 1989. The three magnetograms have the same field of view. As seen in the figures, strong sheared transverse fields are concentrated near the neutral line and they form a global clockwise winding pattern. In Paper I, an account is given of the magnetic nonpotentiality parameters used in this study. The vertical current density is presented in Figure 2. The vertical current density kernels persisted, with little change of configuration, over the whole observing span. Wang, Xu, and Zhang (1994) and Leka *et al.* (1993) have discussed the important characteristics of these vector magnetic fields and vertical current densities. We tabulate the time variation of magnetic fluxes and total vertical currents of positive and negative signs in Table III. The differences between the absolute values of the positive and negative quantities are within a few percent. As seen in the table, the magnetic fluxes and total vertical currents of both signs decreased with time. It is observed that several small δ sunspots (A1, A2 and A3 in Fig. 1a) disappeared in Figure 1b, which suggests that flaring events between Oct. 20 and 21 should be associated with flux cancellation. It is to be noted that there were no remarkable flux emergence during the observing period.

Figure 3 shows the angular shear multiplied by transverse field strength and Figure 4 shows the shear angle multiplied by total field strength. As seen in the figures, strong magnetic shear is concentrated near the inversion line, where H_{β} emission patches were observed (see

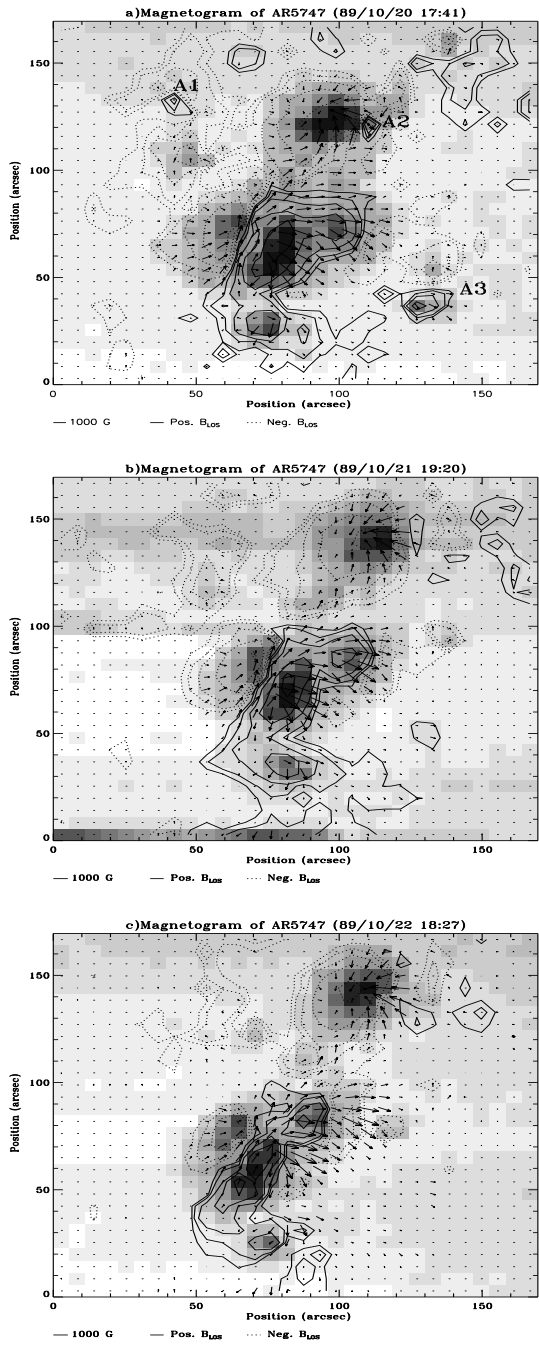


Figure 1. Three MSO vector magnetograms of AR 5747 superposed on white light images taken on Oct. 20–22, 1991. In all the figures, the solid lines stand for positive polarities and the dotted lines for negative polarities. The contour levels correspond to 100, 200, 400, 800 and 1600 G, respectively. The length of arrows represents the magnitude of the transverse field components.

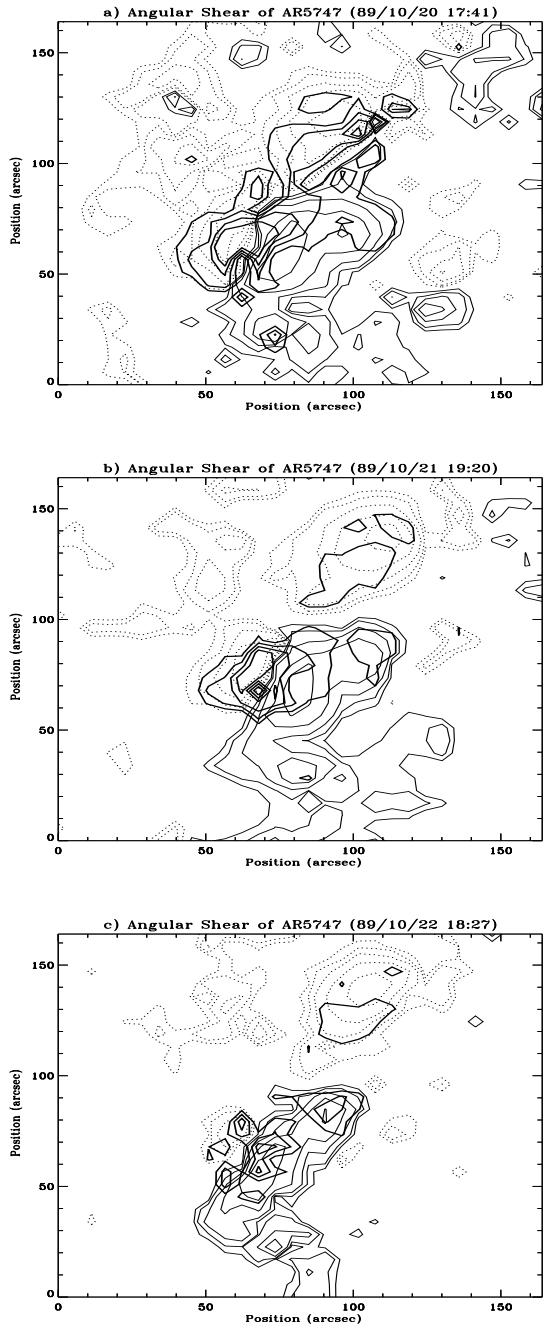


Figure 3. Contours of angular shear multiplied by transverse field strength drawn in thick solid lines are superposed on longitudinal magnetograms. The contour levels are 4.0×10^4 , 7.0×10^4 , 1.0×10^5 and 1.3×10^5 G deg, respectively. In all the panels, the solid lines stand for positive longitudinal polarities and the dotted lines for negative ones. The contour levels in the magnetograms correspond to 100, 200, 400, 800 and 1600 G, respectively.

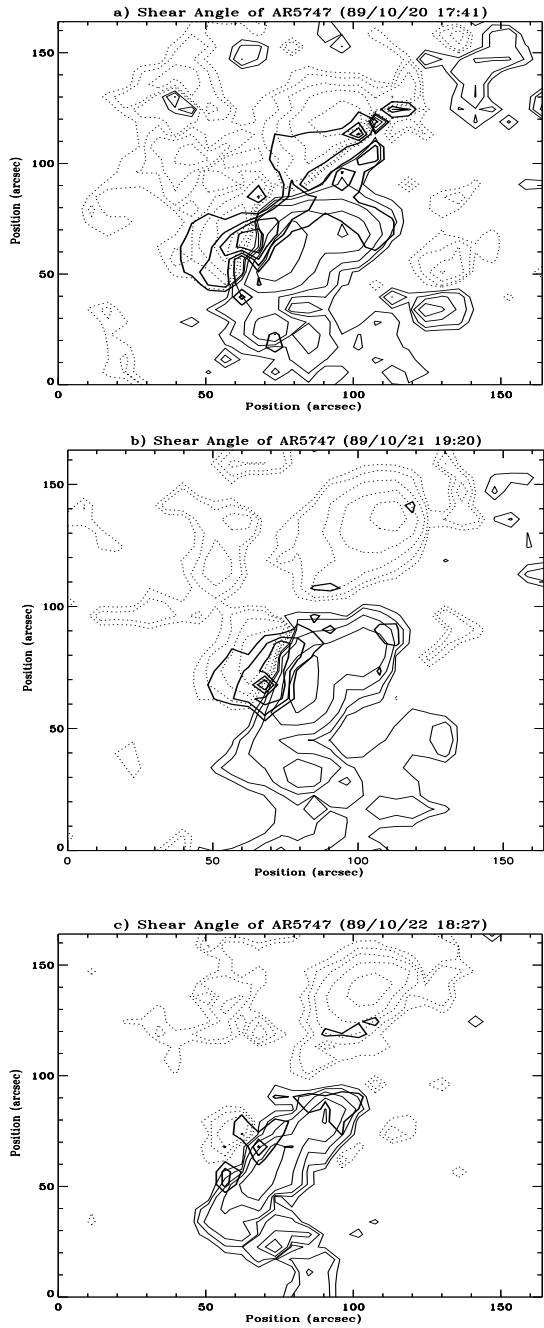


Figure 4. Contours of shear angle multiplied by field strength drawn in thick solid lines are superposed on longitudinal magnetograms. The contour levels are 4.0×10^4 , 7.0×10^4 , 1.0×10^5 and 1.3×10^5 G deg, respectively. The magnetograms are the same as in Figure 3.

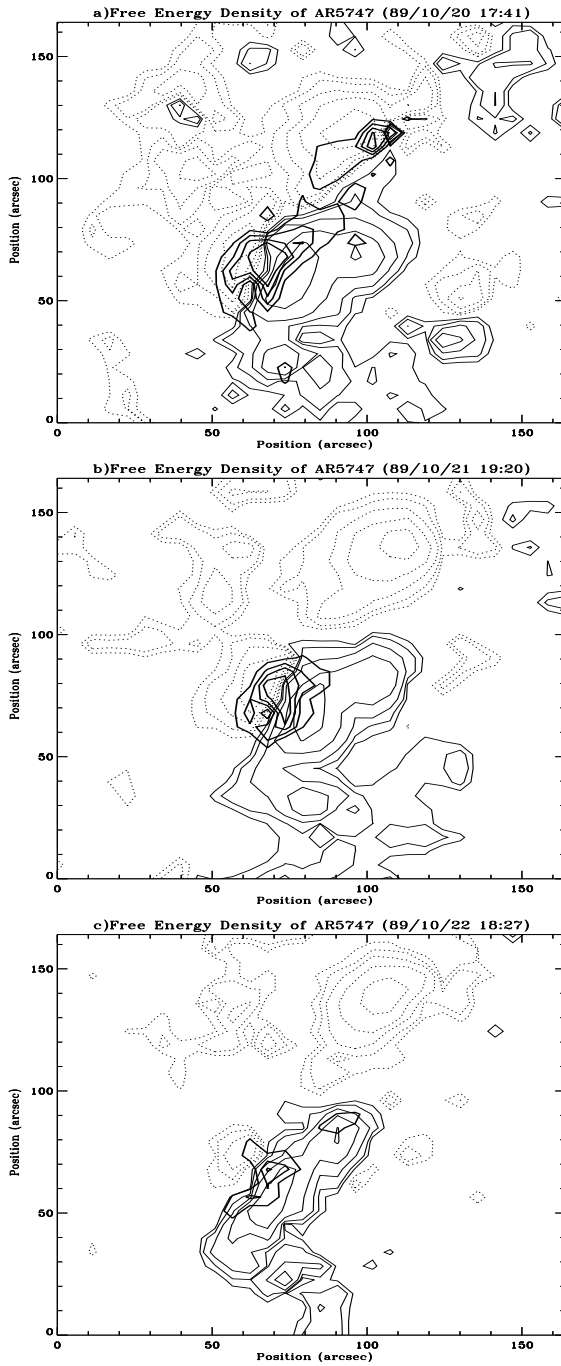


Figure 5. Contours of free energy density drawn in thick solid lines are superposed on magnetograms. The contour levels are 5.0×10^4 , 1.0×10^5 , 1.5×10^5 , 2.0×10^5 and 2.5×10^5 erg/cm³, respectively. The magnetograms are the same as in Figure 3.

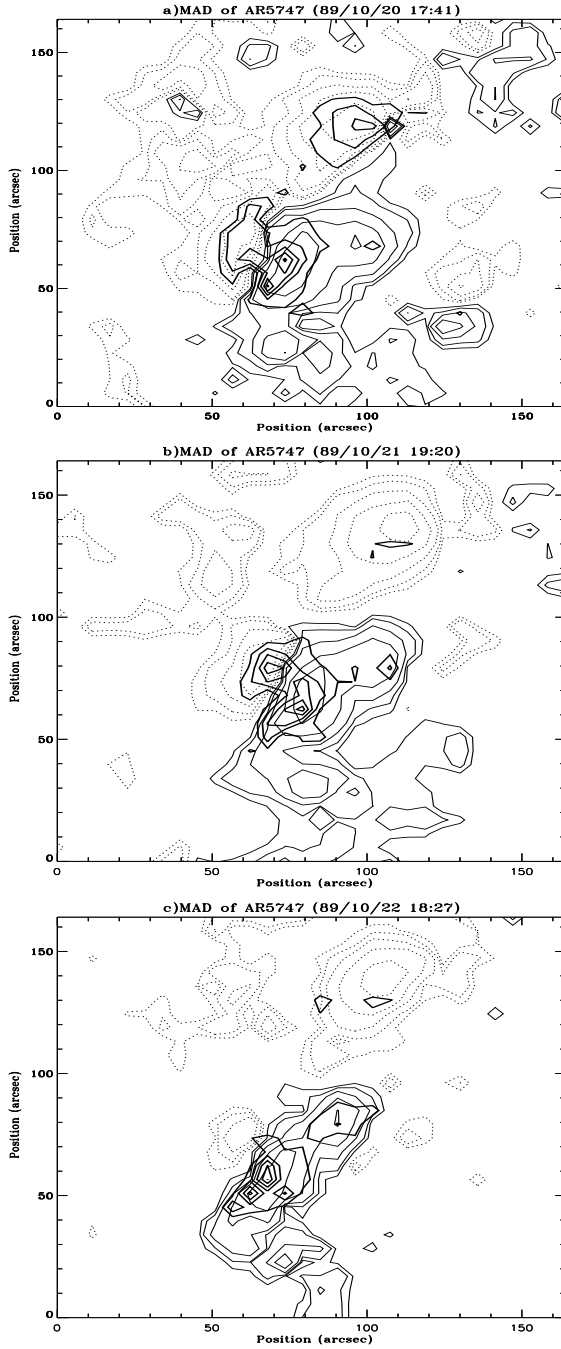


Figure 6. Contours of MAD multiplied by field strength drawn in thick solid lines are superposed on longitudinal magnetograms. The contour levels are 3.0×10^4 , 5.0×10^4 , 7.0×10^4 , 9.0×10^4 and 1.1×10^5 G deg, respectively. The magnetograms are the same as in Figure 3.

Table III. Magnetic fluxes and total vertical currents in AR 5747 for three different times in the observing period. Here σ_J denotes the standard deviation of the vertical current distribution.

Data	Flux(+) [Mx]	Flux(-) [Mx]	$\sum J_z^+$ [A]	$\sum J_z^-$ [A]	σ_J [mA/m ²]
a)	1.56E22	1.51E22	6.7E4	6.6E4	1.4
b)	1.31E22	1.28E22	4.2E4	4.2E4	1.2
c)	0.92E22	0.89E22	3.9E4	4.0E4	1.2

Table IV. Field strength weighted mean magnetic shear angle $\bar{\theta}_s$, transverse field weighted angular shear $\bar{\theta}_a$, mean free energy density $\bar{\rho}_f$, planar sum of magnetic free energy density $\sum \rho_f$, and $\sum(\text{MAD} \times |\mathbf{B}|)$ for AR 5747 for three different times. The values in parentheses are obtained employing the potential field method.

Data	$\bar{\theta}_s$	$\bar{\theta}_a$	$\bar{\rho}_f$	$\sum \rho_f$	$\sum(\text{MAD} \times \mathbf{B})$
a)	46.8(38.4)	71.8(56.1)	2.7(2.0)E4	1.4(1.0)E24	4.7E6
b)	41.3(36.3)	63.0(53.4)	2.1(1.6)E4	9.3(6.9)E23	3.5E6
c)	36.1(32.6)	55.7(48.3)	1.7(1.4)E4	5.1(4.3)E23	2.3E6

Fig. 2 of Wang, Xu, and Zhang 1994). The time variation of two weighted mean shear angles is given in Table IV. The values of two shear angles monotonically decreased with time. The magnetic free energy density is shown in Figure 5. Its evolutionary trend is quite similar to that of shear angles. The 2-D MAD multiplied by total field strength (Figure 6) also has a similar evolutionary pattern to that of the other nonpotentiality parameters above. We summarize the variations of mean free energy density, planar sum of free energy density, and sum of MAD multiplied by field strength in Table IV, in which the values obtained with the potential field method for the 180° ambiguity resolution are also given in parentheses for comparison. As seen in the table, all the nonpotentiality parameters under consideration decreased with time, which suggests that the active region was in a relaxation stage during the observing period.

From the above results, we may infer that the flares that occurred in our observation are just bursty parts of energy release in a long term relaxation of the stressed magnetic field. In a self-organizing system, a transition toward a lower energy state proceeds very mildly in the beginning and for most of time until a sudden bursty event develops as in an avalanche. Why, then, did a series of flares occur, rather than one?

Flares can surely take place in repetition if enough energy is supplied into the system between the flaring events to recover the free energy released by the preceding flaring event. However, this is not the case as far as the flares in our observation are concerned. No indication of energy input, whether flux emergence or increase of magnetic shear, was detected throughout our observing span. We thus speculate that the occurrence of a series of flares was possible due to the complex geometry of our active region magnetic field. A simple bipolar magnetic field would proceed to a lower energy state by one bursty event of reconnection. However, in a complex active region containing more than a pair of magnetic poles, the transition to the lowest energy state may possibly comprise several steps of macroscopic change in field topology. This speculation, of course, has to be examined by further studies involving many other observations and numerical experiments as well.

4. Magnetic Forces and Linear Force-Free Field Approximation

It is generally believed that solar magnetic fields are force-free in the corona, but far from it in the photosphere. However, to construct a force-free model of the coronal magnetic field, the field data observed at the photospheric level are employed as boundary conditions. Not only because a magnetohydrostatic equilibrium under gravity is more difficult to construct than a force-free solution, but also because no reliable information about plasma pressure is available in the photosphere, force-free field modeling with photospheric boundary conditions is being widely attempted (e.g., McClymont and Mikić, 1994 for AR 5747) despite the afore-mentioned inconsistency. The reliability of such models thus depends on how much the field behaves like a force-free field near the photosphere. In this section, we investigate the “force-freeness” of AR 5747.

A force-free field is a magnetic field satisfying the Lorentz force-free condition

$$(\nabla \times \mathbf{B}) \times \mathbf{B} = 0, \quad (1)$$

which can be rewritten as

$$\nabla \times \mathbf{B} = \alpha \mathbf{B}. \quad (2)$$

The so called force-free coefficient α is thus given by

$$\alpha = \frac{J_x}{B_x} = \frac{J_y}{B_y} = \frac{J_z}{B_z}, \quad (3)$$

in rationalized electromagnetic units. Taking divergence of Equation (2) and using $\nabla \cdot \mathbf{B} = 0$, we have

$$\mathbf{B} \cdot \nabla \alpha = 0, \quad (4)$$

which means that α is a function of each field line. With the vector magnetogram of Oct. 20, 1989, Canfield *et al.* (1991) examined whether the ratio of current density to field strength (J/B) is conserved along each elementary flux tube. Although the force-free coefficient $\alpha = J_i/B_i$ is necessarily constant along each field line in a force-free field, the condition is in practice difficult to check due to the noises in current density in weak field regions (McClymont, Jiao, and Mikić, 1997). To examine the force-freeness of AR 5747, we have computed the integrated Lorentz force components scaled with the integrated magnetic pressure force, i.e., F_x/F_o , F_y/F_o and F_z/F_o (Metcalf *et al.* 1995), in which

$$F_x = -\frac{1}{4\pi} \int B_x B_z dx dy, \quad (5)$$

$$F_y = -\frac{1}{4\pi} \int B_y B_z dx dy, \quad (6)$$

$$F_z = -\frac{1}{8\pi} \int (B_z^2 - B_x^2 - B_y^2) dx dy, \quad (7)$$

and

$$F_o = \frac{1}{8\pi} \int (B_z^2 + B_x^2 + B_y^2) dx dy, \quad (8)$$

where F_o is the integrated magnetic pressure force. In this calculation, only pixels with field strength larger than 100 G for both longitudinal and transverse fields are considered to reduce the effect of noise. In Table V, we present the normalized integrated forces obtained from three vector magnetograms. The absolute values of these forces are much smaller than those at the photospheric level of Metcalf *et al.* (1995), which implies that our active region field is more or less force-free even near the solar surface. It is also noted that the magnetic fields of AR 5747 become less force-free in a relaxation stage as times go.

Now we turn to the question whether our active region field is approximately linearly force-free. In Figure 1, the transverse field vectors show a common curling pattern for each magnetic polarity, which allows us to expect that values of the force-free coefficient do not diverge much. To investigate the linearity, we have plotted for each data set B_z vs. J_z and a plausible regression line obtained by eye fitting in Figure 7. The figures show that there exist approximate linear relationships between B_z and J_z for three vector magnetograms. We have already observed in

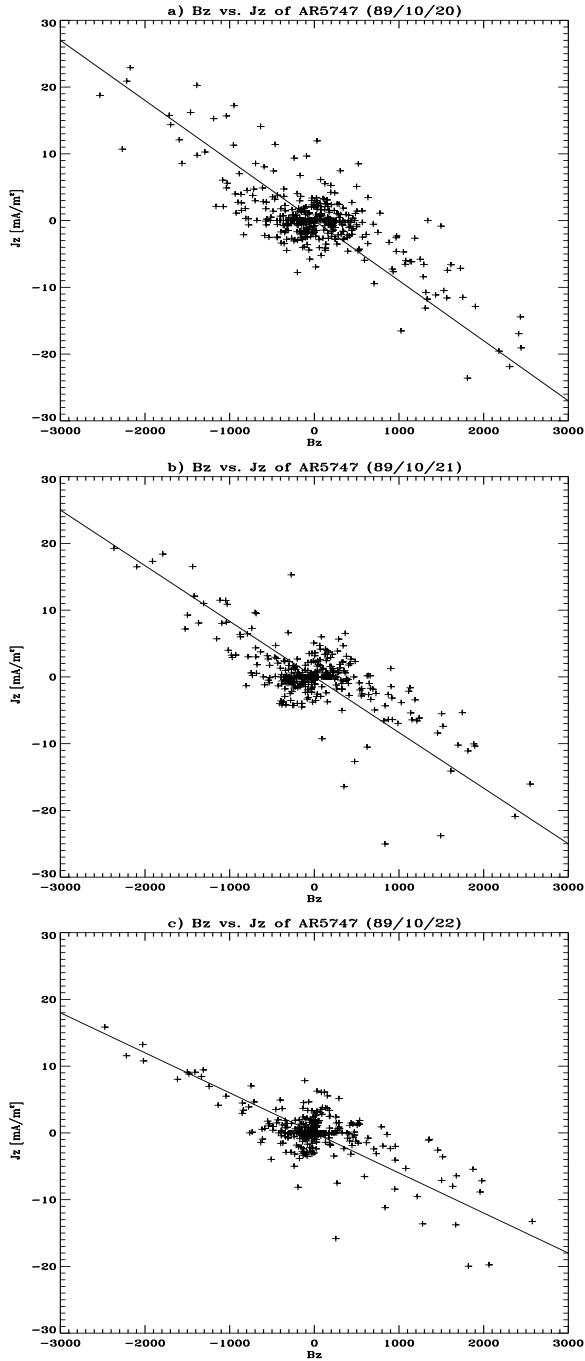


Figure 7. J_z vs. B_z from three vector magnetograms of AR 5747. Straight lines are the regression lines obtained from eye fitting.

Table V. Normalized integrated forces and linear force free coefficients for AR 5747.

Data	F_x/F_o	F_y/F_o	F_z/F_o	$\alpha[\text{m}^{-1}]$	α^*
a)	0.008	0.005	-0.126	-1.1×10^{-7}	-6.8×10^{-8}
b)	0.042	0.015	-0.148	-1.0×10^{-7}	-6.1×10^{-8}
c)	0.097	0.085	-0.222	-7.2×10^{-8}	-4.5×10^{-8}

Asterisked (*) values are obtained by minimizing the difference between the horizontal components of the constant α force-free model and the observed horizontal magnetic fields, considering only pixels with $B_t > 300$ G (Pevtsov *et al.* 1996).

Figures 1 and 2 that the distribution of vertical electric current density well matches that of magnetic fluxes of opposite polarity. In Table V, we have tabulated linear force-free coefficients obtained by linear regression in Figure 7. We have also listed the coefficients obtained by minimizing the difference between the horizontal components in a constant α force-free field model and the horizontal field vectors in the vector magnetogram, considering only pixels with $B_t > 300$ G (Pevtsov *et al.*, 1996). In both sets, the absolute value of force-free coefficients decreased with time, as other nonpotentiality parameters did. This suggests that the linear force-free coefficient could be as good a nonpotential evolutionary indicator as other nonpotentiality parameters as long as the linear force-free approximation is more or less valid. Furthermore, the linear force-free coefficient has a merit as a global parameter.

5. Summary and Conclusion

In this study, we have analyzed the MSO vector magnetograms of AR 5747 taken on October 20 to 22, 1989. A nonlinear least square method was adopted to derive the magnetic field vectors from the observed Stokes profiles and a multi-step ambiguity solution method was used to resolve the 180° ambiguity. From the ambiguity-resolved vector magnetograms, we have derived a set of physical quantities which are magnetic flux, vertical current density, magnetic shear angle, angular shear, magnetic free energy density and MAD, a measure of magnetic field discontinuity. In order to examine the force-free character of the active region field, we have calculated the normalized integrated Lorentz forces and compared the longitudinal field B_z and the corresponding

vertical current density J_z . Most important results from this work can be summarized as follows.

1) Magnetic nonpotentiality is concentrated near the inversion line, where flare brightenings are observed.

2) All the physical parameters that we have considered (vertical current density, mean shear angle, mean angular shear, sum of free energy density and sum of MAD) decreased with time, which indicates that the active region was in a relaxation period.

3) The X-ray flares that occurred during the observing period could be related with flux cancellation. Flaring events might be considered as bursty parts in the long term relaxation process.

4) It is found that the active region was approximately linearly force-free throughout the observing span and the absolute value of the derived linear force-free coefficient decreased with time. Our result suggests that the linear force-free coefficient could be a good global parameter indicating the evolutionary status of an active region as long as the field is approximately force-free.

Acknowledgements

We wish to thank Dr. Metcalf for allowing us to use some of his numerical routines for analyzing vector magnetograms and Dr. Pevtsov for helpful comments. The data from the Mees Solar Observatory, University of Hawaii are produced with the support of NASA grant NAG 5-4941 and NASA contract NAS8-40801. This work has been supported in part by the Basic Research Fund (99-1-500-00 and 99-1-500-21) of Korea Astronomy Observatory and in part by the Korea-US Cooperative Science Program under KOSEF(995-0200-004-2).

References

- Canfield, R. C., Fan, Y. , Leka, K. D., Lites, B. W., and Zirin, H.: 1991, in *Solar Polarimetry*, Proceeding of the Workshop of Solar Polarimetry, ed. L. November , p. 296.
- Canfield, R. C., La Beaujardiere, J.-F., Han, Y., Leka, K. D., McClymont, A. N., Metcalf, T. R., Mickey, D. L., Wulser, J.-P., and Lites, B. W.: 1993, *Astrophys. J.* **411**, 362.
- Hagyard, M. J., Smith, Jr., J. B., Teuber, D., and West, E. A.: 1984, *Solar Phys.* **91**, 115.
- Hagyard, M. J., Ventkatarishnan, P., and Smith, Jr., J. B.: 1990, *Astrophys. J. Suppl.* **73**, 159.
- Leka, K. D., Canfield, R. C., McClymont, A. N., de la Beaujardiere, J. F., and Fan, Y.: 1993, *Astrophys. J.* **411**, 370.

- McClymont, A. N. and Mikić, Z.: 1994, *Astrophys. J.* **422**, 899.
- McClymont, A. N., Jiao, L., and Mikić, Z.: 1997, *Solar Phys.* **174**, 191.
- Metcalf, T. R., Canfield, R. C., Mickey, D. L., and Lites, B. W.: 1991, in *Solar Polarimetry*, Proceeding of the Workshop of Solar Polarimetry, ed. L. November, p. 376 .
- Metcalf, T. R., Jiao, L., McClymont, A. N., Canfield, R. C., and Uitenbroek, H.: 1995, *Astrophys. J.* **439**, 474.
- Mickey, D. L.: 1985, *Solar Phys.* **97**, 223.
- Moon, Y.-J., Yun, H. S., Lee, S. W., Kim, J.-H. Choe, G. S., Park, Y. D., Ai, G., Zhang, H., and Fang, C.: 1999a, *Solar Phys.* **184**, 323.
- Moon, Y.-J., Park, Y. D., and Yun, H. S.: 1999b, *J. Korean Astron. Soc.* **32**, 63.
- Moon, Y.-J., Yun, H. S., Choe, G. S., Park, Y. D., and Mickey, D. L.: 1999c, submitted to *Solar Physics*. (Paper I)
- Pevtsov, A. A., Canfield, R. C., and Zirin, H.: 1996, *Astrophys. J.* **473**, 533.
- Pevtsov, A. A., Canfield, R. C., and McClymont, A. N.: 1997, *Astrophys. J.* **481**, 973.
- Ronan, R. S., Mickey, D. L., and Orral, F. Q.: 1987, *Solar Phys.* **113**, 353.
- Skumanich, A and Lites, B. W.: 1987, *Astrophys. J.* **322**, 473.
- Wang, H.: 1997, *Solar Phys.* **174**, 163.
- Wang, J., Shi, Z., Wang, H., and Lue, Y.: 1996, *Astrophys. J.* **456**, 861.
- Wang, T., Xu, A., and Zhang, H.: 1994, *Solar Phys.* **155**, 99.